Journal of Materiomics 7 (2021) 219–225

Contents lists available at ScienceDirect

Journal of Materiomics

journal homepage: www.journals.elsevier.com/journal-of-materiomics/

Opinion paper

Nacre-bionic nanocomposite membrane for efficient in-plane dissipation heat harvest under high temperature

Jiemin Wang [a], Dan Liu [a, **], Quanxiang Li [a], Cheng Chen [a], Zhiqiang Chen [a], Minoo Naebe [a], Pingan Song [b, ***], David Portehault [c], Christopher J. Garvey [d], Dmitri Golberg [e], Weiwei Lei [a, *]

[a] Institute for Frontier Materials, Deakin University, Waurn Ponds Campus, Locked Bag 20000, Victoria, 3220, Australia
[b] Center for Future Materials, University of Southern Queensland, Toowoomba, 4350, Australia
[c] Sorbonne Université, CNRS, Laboratoire de Chimie de La Matière Condensée de Paris (CMCP), 4 Place Jussieu, F-75005, Paris, France
[d] Australia Nuclear Science and Technology Organization (ANSTO), Sydney, New South Wales, 2232, Australia
[e] Centre for Materials Science and School of Chemistry and Physics, Queensland University of Technology (QUT), Brisbane, QLD, 4001, Australia

ARTICLE INFO

Article history:
Received 29 April 2020
Received in revised form
4 August 2020
Accepted 17 August 2020

Keywords:
Boron nitride nanosheets
Nanocomposite membrane
Nacre-biomimetic
High temperature heat spreader
In-plane dissipation heat

ABSTRACT

Waste heat management holds great promise to create a sustainable and energy-efficient society as well as contributes to the alleviation of global warming. Harvesting and converting this waste heat in order to improve the efficiency is a major challenge. Here we report biomimetic nacre-like hydroxyl-functionalized boron nitride (BN)-polyimide (PI) nanocomposite membranes as efficient 2D in-plane heat conductor to dissipate and convert waste heat at high temperature. The hierarchically layered nanostructured membrane with oriented BN nanosheets gives rise to a very large anisotropy in heat transport properties, with a high in-plane thermal conductivity (TC) of 51 W m^{-1} K^{-1} at a temperature of ~300 °C, 7314% higher than that of the pure polymer. The membrane also exhibits superior thermal stability and fire resistance, enabling its workability in a hot environment. In addition to cooling conventional exothermic electronics, the large TC enables the membrane as a thin and 2D anisotropic heat sink to generate a large temperature gradient in a thermoelectric module ($\Delta T = 23$ °C) through effective heat diffusion on the cold side under 220 °C heating. The waste heat under high temperature is therefore efficiently harvested and converted to power electronics, thus saving more thermal energy by largely decreasing consumption.

1. Introduction

Recent years have witnessed the growing power density of electronic devices, which results in excessive thermal energy accumulation. The concomitant temperature increase can damage the products and even raise safety risks, such as fire or explosion [1]. Other sources of heat, like furnaces in steel factories also generate large amounts of waste heat that is directly released into the surrounding atmosphere. Heat dissipating materials are usually required to enable the cooling of these electronics and furnaces [2,3]. In this context, hexagonal boron nitride (BN) nanosheets-based heat sinks have been largely investigated owing to the high thermal conductivity (TC) and chemical stability [4–8]. BN based nanocomposites can also be conveniently processed as a flexible membrane to optimize conformal coating of the heat source, and then fasten heat diffusion from the hot source to the membrane edges along the in-plane direction, thereby decreasing the hot source temperature and dissipating the accumulated heat. This cooling process, however, gives rise to a waste of excessive dissipated thermal energy. Despite great advances in the development of heat harvest thermoelectric devices, they are restricted to operation at relatively low-grade temperatures (< 100 °C) [9]. Therefore, the design of high-performance thermally conductive membranes remains a major challenge to dissipate as well as efficiently harvest high-temperature waste heat above 200 °C.

* Corresponding author.
** Corresponding author.
*** Corresponding author.
E-mail addresses: dan.liu@deakin.edu.au (D. Liu), pingansong@gmail.com (P. Song), weiwei.lei@deakin.edu.au (W. Lei).
Peer review under responsibility of The Chinese Ceramic Society.

https://doi.org/10.1016/j.jmat.2020.08.006

Due to its structural configuration, the most efficient way to conduct heat within a membrane is to maximize the in-plane TC while maintaining low transverse TC, hence achieving a large TC anisotropic ratio. Previous researches have reported BN/polymer nanocomposite membranes with biomimetic nacre-like structure for effective thermal diffusion [4,5,7,8,10,11]. The nacre-like laminated structure is based on the lateral alignment of platelets within a polymer matrix in a "brick-and-mortar" scheme. It enables heat conduction along the nanosheet layers, resulting in large in-plane thermal conductivity. The nacre mimics membranes also exhibit flexibility and toughness, fully applicable to soft electronics. However, the low thermal stability and moisture sensitivity of polymers such as poly vinyl alcohol (PVA) [4,10,11], poly diallyldimethylammonium chloride (PDDA) [5] and cellulose [7,8] have hindered the practical use to these membranes above 200 °C and in humid atmosphere. Some thermostable polymers such as polyimide (PI) have been considered to reach higher temperatures [12,13]. Nevertheless, to date, nacre-like nanocomposites based on BN and PI remain intractable to achieve *via* vacuum filtration (VAF) because of the poor compatibility between BN and PI as well as the poor solubility of PI in water. Moreover, traditional mixing and coating methods result in relatively low in-plane thermal conductivity [12,13]. Overall, no thermally conductive yet electrically insulating nacre-like membrane has been delivered to operate in harsh temperature conditions, above 200 °C, with satisfying high thermal conductivity (>30 W m^{-1} K^{-1}). Hence, the design of nacre-like BN/PI nanocomposites membranes is critical to combine high thermal conductivity and thermal stability.

Here, we design freestanding and nacre-like BN nanosheet/PI (BN-PI) nanocomposite membranes by using the VAF assembly of hydroxyl functionalized BN nanosheets and a water-soluble modified precursor of PI, followed by thermal treatment. Besides significant improvements in mechanical performances and flame resistance, the membranes exhibit considerable in-plane TCs at 200 °C (35–49 W m^{-1} K^{-1}) and at 300 °C (36–51 W m^{-1} K^{-1}) with 30–70 wt% BN, respectively, allowing efficient anisotropic thermal regulation in a wide temperature range. In order to dissipate and harvest the redundant heat, the membrane was connected to the cold side of a thermoelectric (TE) module. Unlike conventional exothermic electronics with low heating temperature (<100 °C), the TE module can be heated to maximum 220 °C, thereby benefiting our membrane for cooling applications from high temperatures. Thanks to the ability of the BN-PI membrane to act as an efficient and thermo-stable heat sink through in-plane heat conduction, the TE module could reach larger temperature gradient (ΔT) between the hot and cold sides, and achieve larger thermoelectric energy conversion efficiency with more thermal energy conservation. This work then offers an original methodology to design a biomimic thermo-anisotropic membrane as high temperature heat spreader for cost-effective harvesting and conversion of waste heat.

2. Experimental

2.1. Material synthesis

Preparation of functional boron nitride (BN) nanosheets. At first, h-BN (Momentive Performance Materials, Inc.) and D-glucose (Sigma-Aldrich) were mixed and milled in a planetary ball mill (Pulverisette 7, Fritsch) at a rotation speed of 500 r.p.m. for 20 h. The achieved powders were dissolved in water and dialyzed for 7 days to remove the D-glucose, producing stable aqueous dispersions of BN nanosheets [14].

Preparation of water-soluble polyimide (PI) precursor. The 4, 4′-diaminodiphenyl ether (4,4′-ODA, Sigma-Aldrich), pyromellitic dianhydride (PMDA, Sigma-Aldrich) and triethylamine (TEA) (Sigma-Aldrich) were used to synthesize (amic acid) (PAA) solution, as previously reported [6,15].

Preparation of freestanding BN-PI membranes. BN-PI membranes were fabricated by water vacuum-assisted filtration and thermal crosslinking. The aqueous solution of BN nanosheets was mixed with PAA solution at first, and then the mixtures were magnetically stirred for 1 h. Then the mixtures were filtered under vacuum. These BN-PAA membranes can be readily peeled off from the polyethylene membrane and retain their freestanding state. After these procedures, the films were thermally cross-linked in a tube furnace under N_2 protection at 80 °C, 150 °C, 170 °C for 1 h, respectively, and finally at 300 °C for 2 h.

2.2. Material characterization

XRD measurements were processed on a PANalytical X'Pert apparatus with Cu Kα radiation. The FTIR spectra were measured using a Nicolet 7199 FTIR spectrometer. XPS analysis was performed on an Kratos AXIS Nova instrument with Al Kα X-ray as the excitation source. SEM imaging was carried out using a Zeiss Supra 55 VP SEM instrument. TEM and HRTEM imaging was conducted on a JEOL 2100F microscope operating at 200 kV. The mechanical measurements were performed by means of an Instron 30 KN tensile tester on a 50 N load cell with a loading rate of 5 mm/min. The modeling was processed by COMOSOL Multiphasics software under steady-state. The thermal weight losses were measured using TGA on a TA Instruments Q50 at a heating rate of 10 °C min^{-1} from room temperature to 800 °C under air flow. The specific heat was measured by using the differential scanning calorimetry (DSC Q200, TA Instruments). Here, the heat capacity of a nanocomposite was calculated using the equation: $C_p = C_{pf}\Phi + C_{pm}(1-\Phi)$ [4–6], where C_p is the specific heat capacity of the nanocomposite and C_{pf} is the specific heat capacity of the filler (BN), and C_{pm} is the specific heat capacity of the polymer (PI), whereas Φ represents the volume fraction of BN. The in-plane and out-of-plane thermal diffusivity of nanocomposite membranes were measured from 30 to 300 °C with an LFA 457 analyzer (NETZSCH, Germany). The thermal conductivites of the nanocomposite membranes were calculated according to the equation $TC = \alpha \times \rho \times C$ (Table S2), where α, ρ, and C correspond to the thermal diffusivity, density, and specific heat capacity of the nanocomposites. The flame retardancy test was performed on BN-PI and pure PI membranes separately. The fire from a gas burner was applied to the tested membranes for 60 s and then removed. The thermoelectric (TE) measurements were performed by placing the membrane on the cold side surface of a commercial TE module (30 mm × 30 mm, 128 pairs of p-n junction with Bi_2Te_3 as materials). Then, a thermal conductive glue (TC~4.5 W m^{-1} K^{-1}) was coated on the cold side of TE module to paste the membrane. Meanwhile, the TE module was also placed on a Cu column with hot stage heating. The voltage and current values were measured by a multimeter and the temperatures of cold side and hot side were detected by 2 digital thermometers. The maximum heating temperature was not more than 220 °C, otherwise the TE module would malfunction due to high temperature.

3. Results and discussion

The fabrication of the membranes is illustrated in Fig. 1a. Firstly, hydroxylated BN nanosheets (OH-BN) were produced by ball milling (Fig. S1a) [14]. These BN nanosheets possess 100–300 nm lateral size, 1–2 nm thickness and hydroxyl-functionalized surfaces, which enable water dispersibility (Figs. S1b–e), hence facilitating the vacuum filtration processing. Secondly, we prepared the aqueous solution of polyamic acid (PAA), the precursor of polyimide PI [15]. The BN suspension and aqueous solution of PAA were then

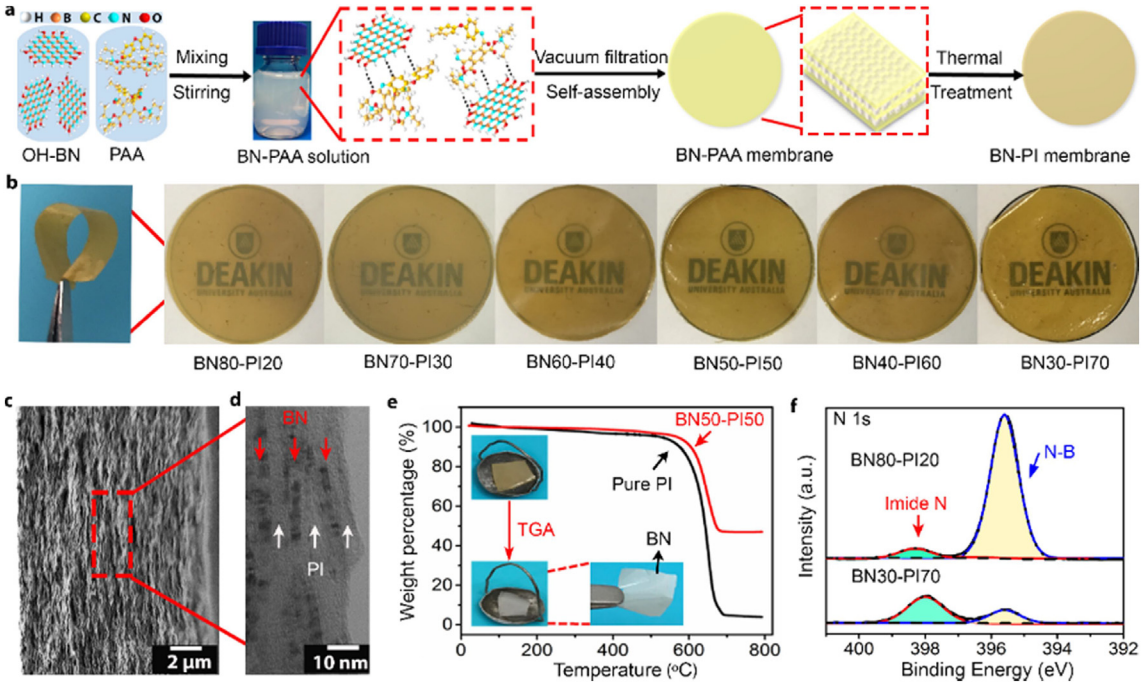

Fig. 1. Fabrication and structural characterization of nacre-like BN-polyimide nanocomposite membranes. (a) Scheme of the fabrication process of the membranes. (b) Optical images of the membranes with different BN weight loadings. The use of the logo is permitted from the Institute of Frontier Materials, Deakin University. (c) SEM and (d) TEM images of the cross-sectional morphology of a BN50-PI50 membrane. (e) TGA traces of BN50-PI50 and pure PI membranes. The insets in (e) display the optical images of the nanocomposite membrane before and after TGA tests. (f) N 1s region of the XPS spectra of BN80-PI20 and BN30-PI70.

mixed at arbitrary ratios to form a homogeneous mixture without visible aggregation. We assume that multiple nanosheets-polymer interactions may arise, such as hydrogen-bonding, π-π stacking, and electrostatic repulsions, and then pack the BN sheets and PAA in water. Afterwards, the yellowish suspension was obtained (Fig. S2). The final free-standing yellow BN-PI nanocomposite membranes were readily prepared by VAF followed by thermal treatment. BN-PI nanocomposite membranes with various BN contents could be conveniently produced by varying the concentrations of the components in the aqueous suspension. The weight contents of BN evaluated by thermogravimetric analysis (TGA) were consistent with the targeted mass ratios (Fig. S3). These ratios set at 80, 70, 60, 50, 40, and 30 wt% for membranes were denoted as BN80-PI20, BN70-PI30, BN60-PI40, BN50-PI50, BN40-PI60 and BN30-PI70, respectively. As shown in Fig. 1b, the resultant BN-PI membranes are translucent and flexible even at high BN loading, despite the intrinsic brittleness of BN nanosheets [14]. Scanning electron microscopy (SEM) and transmission electron microscopy (TEM) images (Fig. 1c and d) highlight the layered nanostructure of the membrane BN50-PI50. On the surface area, the BN nanosheets are homogeneously distributed within the PI matrix (Fig. S4). Meanwhile, cross-section images confirm the nacre-like lamellar "brick-and-mortar" structure (Fig. 1c-d and Fig. S5). As shown in Fig. 1e inset, the white BN membranes maintain their original shape even after experiencing heat treatment from 25 °C to 800 °C in air, thus indicating excellent structure stability and thermal stability. The SEM images of the net BN membrane (Fig. S6) after calcination show the parallel stacking of BN lamellae with PI burnt-out spaces, providing another evidence for the layered self-assembly of the nanocomposite membrane. The chemical composition was investigated by X-ray photoelectron spectroscopy (XPS) (Fig. 1f and Fig. S7). The N-B peak (~398 eV, Fig. 1f) [14] dominates in the BN80-PI20 membrane, while the relatively strong imide N peak (~400.5 eV, Fig. 1f) [15,16] appears in the BN30-PI70 in the N 1s spectrum, confirming the ability to tune the ratio between BN and PI. The results are further evidenced by X-ray diffraction (XRD) (Fig. S8a), small-angle X-ray scattering (SAXS) (Fig. S8b) and Fourier transform infrared spectroscopy (FTIR) (Fig. S9).

The mechanical properties of the nanocomposite membranes were then investigated (Fig. 2a, Fig. S10 and Table S1). The BN50-PI50 membrane exhibits the maximum tensile stress with a value of ~140 MPa and a Young's modulus of ~2.53 GPa (Fig. S10 a, b and c). These values are superior to those of BN-PVA and BN-PDDA membranes reported previously [4,5]. The enhancement of the mechanical properties of the materials shown herein may arise from both the superior mechanical characteristics of PI and the homogeneous distribution of the BN nanosheets. Under tensile loads, the artificial nacre-like architecture enables longitudinal transfer of the force along the nanosheets and through the polymer component, which then jointly undertake the load [17–21]. Not surprisingly, the mechanical properties are optimized for an intermediate BN content, here for BN50-PI50 at 50 wt % BN. Below this amount, the BN sheets are not in sufficient amount to enhance the mechanical properties, whereas an excessive BN content can lead to reduced extensibility and toughness (Fig. S10d). We then measured the thermal conductivity properties. As expected, the in-plane TC increases with the BN content (Fig. 2b), leading to a value of 47.8 W m^{-1} K^{-1} for BN70-PI30. Even at a low 30 wt % (17.7 vol%) BN loading (BN30-PI70 membrane), the in-plane TC is enhanced with a value as high as 32.1 W m^{-1} K^{-1}, about 7314% increase compared to the pure polymer. In contrast, the out-of-plane TC values maintain small values. Therefore, the high in-plane thermal conductivity of the BN nanosheets is attributed to the nacre-like structure: the aligned sheets build a heat path allowing rapid heat dissipation in-plane rather than out-of-plane, resulting in a significant thermal anisotropy [4,5,22–24]. To compare the thermal and mechanical properties, we plotted both tensile stress and in-plane TCs in a performance chart in Fig. 2c. Notably, for all BN

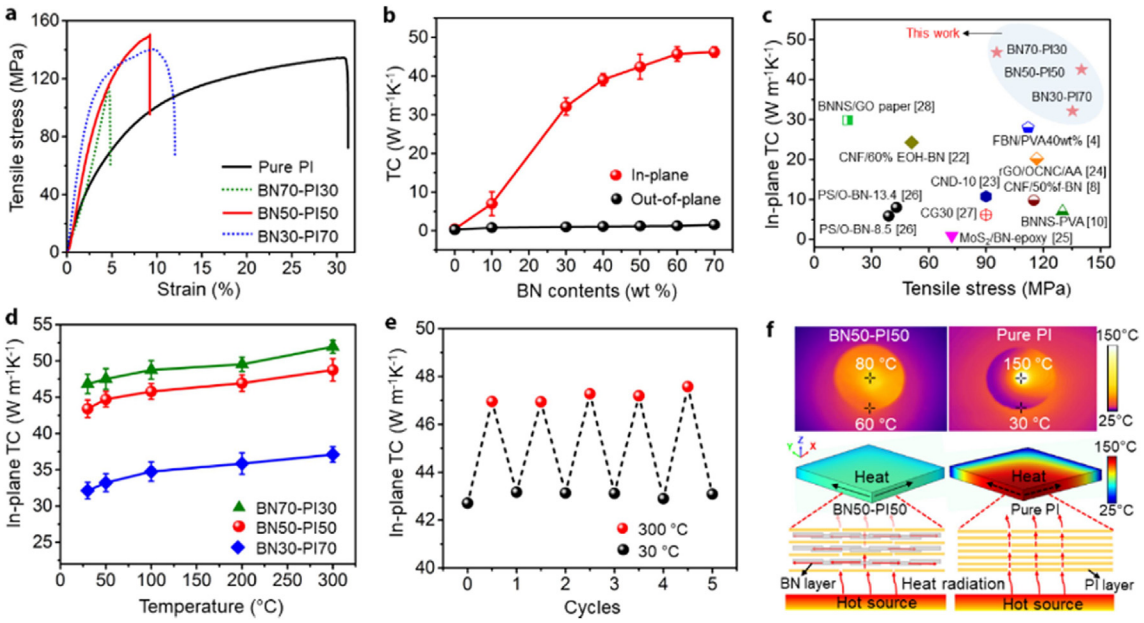

Fig. 2. Mechanical and thermal conduction properties of the BN-PI membranes. (a) Tensile stress measurements. (b) In-plane and out-of-plane thermal conductivities (TCs) with different BN weight loadings. (c) Performance chart of membranes integrating in-plane TC and tensile stress. (d) Temperature-dependent TCs of BN-PI membranes. (e) Temperature cyclability of the BN50-PI50 membrane. (f) In-plane heat dissipation mechanism (IR imaging and steady simulation model) of BN-PI membrane (left) and pure PI membrane (right).

contents from 30 wt% to 70 wt%, the BN-PI membranes show superior thermal conduction and mechanical properties than other membranes based on BN and other 2D materials, such as graphene and MoS_2 [4,8,10,22–28]. In addition, the highest temperatures that membranes can withstand determine their practical applications in hot environments. However, previously reported polymer/BN composites cannot maintain their thermal conductivity above 125–160 °C [4,5,7,8,10,11]. Impressively, the BN-PI membranes described herein retain large TCs at temperatures up to 300 °C (36–51 W m^{-1} K^{-1} with 30–70 wt% BN loading) (Fig. 2d). Regardless of subtle fluctuations due to the balance effect of Umklapp phonon scattering and reduced Kapitsa resistance [7], the TC measured for the BN-PI membranes increases by less than 10% from 30 °C to 300 °C, thus showing stable enough thermal properties for applications at high temperatures. Furthermore, TC shows only a slight change upon 5 heating/cooling alternative cycles between 30 °C and 300 °C (Fig. 2e), demonstrating high cycle durability.

To further understand the heat conduction mechanism, an infrared (IR) thermal camera was employed to record the temperature distribution in the membrane in a steady-state condition (Fig. 2f). The BN50-PI50 membrane with optimal mechanical and thermal performances was chosen for these measurements. The membrane was put on a hot iron head at 200 °C. A blurry hot spot appears with low temperature on its surface centre (80 °C). Moreover, the temperature is also uniformly distributed from the centre to the edge of the membrane (60 °C). On the contrary, the pure PI membrane shows a focused bright spot in its centre, reaching 150 °C, while the edge temperature is as low as 30 °C. The high in-plane TC and large thermal conductive anisotropy of the BN-PI membrane enable the heat flux to rapidly spread from the hot spot to the edge along the in-plane direction, leading to efficient cooling with a uniform temperature distribution. Steady-state simulations also confirm the homogeneous temperature distribution within the BN50-PI50 membrane, originating from efficient in-plane heat dissipation (Fig. S11). Whereas intensive heat accumulates in the centre for the pure PI membrane, causing a strong temperature gradient.

To further verify the anisotropic thermal property, the anisotropic thermal conduction ratios ($TC_{in\text{-}plane}/TC_{out\text{-}of\text{-}plane}$) among various heat sink materials are displayed in Fig. 3a. Obviously, BN50-PI50 possesses a large anisotropic ratio of 42, which is greater than that for graphite/polymer, CNT/polymer composites and metallic wood [29–32]. Besides, the nanocomposite membrane with the lamellae-based, nacre-like structure has a greater anisotropy than films prepared *via* blade coating [7,8,13]. This result shows that the bio-inspired construction can orient the phonon transport by aligning the thermally conductive BN sheets along the plane of the membrane. Therefore, the in-plane BN lamellae not only determines the great mechanical property but also guarantees the excellent anisotropic thermal conduction performances. Furthermore, we also compared the TC values during a wide temperature range (25–300 °C) with different BN contents (Fig. 3b). It is important that the BN-PI membranes presented large TC values of an order of magnitude higher than other BN-based thermal conductive composites for all temperatures [7,12,13,26,33–36]. In addition, we also observed excellent flame-resistance of the as-designed membranes (Fig. 3c). The pure PI membrane was combustible and burnt out in 5 s when it was close to the flame. Nevertheless, for the nanocomposites, the fire resistance capacity was improved with the BN contents (Fig. S12). When the BN weight content reaches 50 wt% or more, the nanocomposite membranes could maintain their initial shapes within around 1 min. Therefore, such a unique performances combination enables the BN-PI membrane to serve as a promising 2D heat sink for thermal manipulation at high temperature up to 300 °C as well as validating practical workability in some extreme conditions, such as fire circumstances.

In addition to cooling the conventional electronics such as (light-emitting diode) LED bubbles with working temperature less than 100 °C [5–7], the high cooling efficiency of BN-PI membranes could advantageously contribute to the performances of thermoelectric generators (TEGs) at higher temperatures (>200 °C) by using the membranes as heat sinks. In order to achieve great

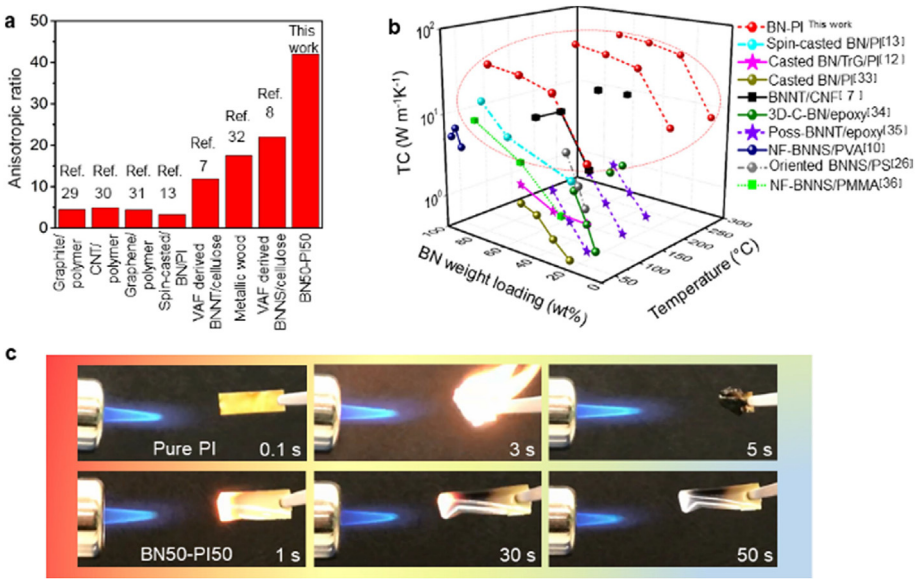

Fig. 3. The high temperature thermo-anisotropy and flame resistance. (a) Comparison of anisotropic thermal conduction ratios among various heat sink materials. (b) Comparison of TCs over a wide temperature range with different BN contents. (c) Flame resistance test between pure PI and BN50-PI50 membrane.

thermal-to-electricity conversion in TEGs, the temperature difference between the cold (T_{cold}) and hot (T_{hot}) ends must be maximized [15,37]. Heat sinks enable maintaining low T_{cold} by dissipating heat. Most of them are composed of metals or carbon materials that are bulky and not electrically insulating. They also tend to generate heat by the photothermal effect, especially when exposed to outdoor environment [38–40]. Therefore, the 2D lightweight BN-PI membranes described herein, with unprecedented combination of large in-plane TCs and high temperature workability, may serve as efficient next-generation heat sinks to harvest waste heat with TEGs. We designed a TEG (Fig. 4a) based on the BN50-PI50 membrane to evaluate the feasibility of heat harvesting and conversion. A large freestanding membrane with diameter of 65 mm was first fabricated (Fig. S13) according to the process described in Fig. 1a. It was then assembled on the cold side of a commercial TE module (30 mm in length and width). The as-obtained TEG was placed on a Cu column (hot source) heated by a hot stage. The whole experiment was conducted in the steady-state achieved after at least 10 min of operation. The corresponding temperature distributions from front and side views of the TEG (without or with membrane loaded) were measured by IR imaging (Fig. 4b). When the temperature of the hot stage reached 220 °C, the central and edge temperatures of the BN50-PI50 membrane were 177 °C and 155 °C, respectively. In contrast, the temperature of the naturally air-cooled device without membrane rose to ~190 °C in the centre. Notably, the pure PI membrane of the same size

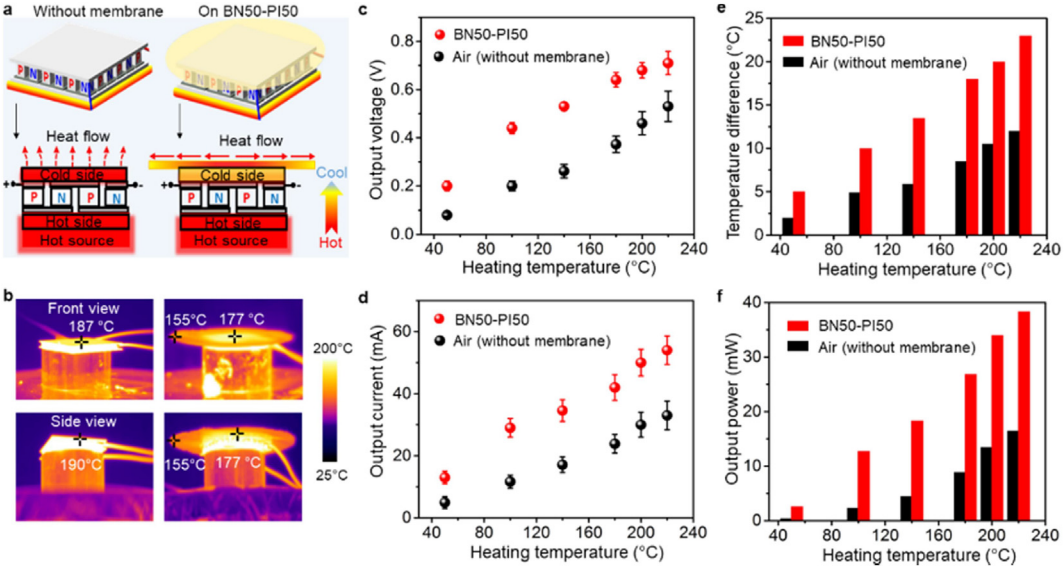

Fig. 4. The applications of BN-PI nanocomposite membranes as a heat sink for thermal energy conversion. (a) Scheme of the design concept and mechanism for natural air-cooled (left) and BN50-PI50 membrane-loaded (right) TE module. (b) Corresponding temperatures recording by IR imaging for 220 °C heating. (c) Voltage generated at different heating temperatures. (d) Current generated at different heating temperatures. (e) Temperature difference between the hot and cold sides of the TEG generators at different heating temperatures. (f) Power generated at different heating temperatures.

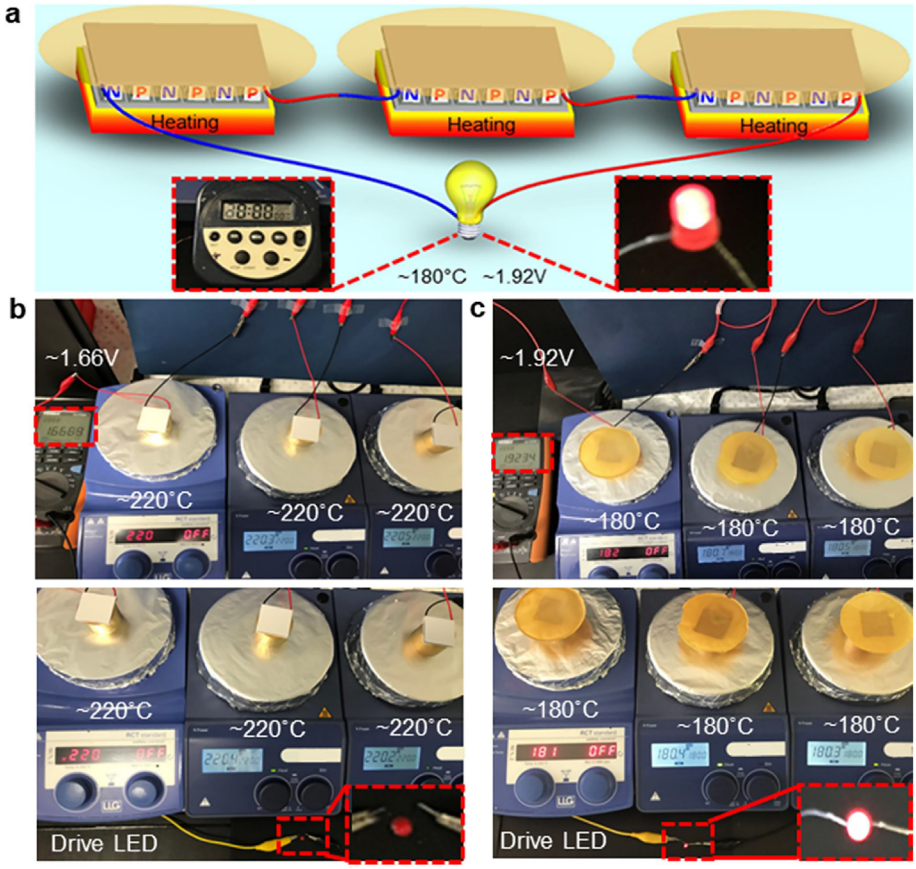

Fig. 5. Tandem connection for practical cooling from high temperature and thermal energy utilization. (a) The scheme of BN50-PI50 for efficient high temperature heat dissipation and practical thermal energy conversion. (b) The optical picture of practical tandem of an air-cooling based TE module. (c) The optical picture of a practical tandem of BN50-PI50 loaded TE module.

showed similar or even higher temperatures under air cooling since the pure polymer membrane is thermo-insulating; this results in the worse heat dissipation under air cooling. [15] Hence, we did not present the results for a pure PI membrane. To further validate this observation, we also used two digital thermometers to detect the temperatures of the cold and hot sides of the TEG (Fig. S14). The temperature gradient expands from 12 °C to 23 °C for the naturally cooled and the membrane-modified device, respectively. Although the temperatures measured by the point-thermometer differ by few degrees from those evaluated by IR imaging, the trends and orders of magnitude are identical: they clearly demonstrate that the BN50-PI50 heat sink membrane effectively dissipates heat and double the temperature gradient. As a result, the thermoelectric conversion efficiency of the TEG should be strongly increased. Fig. 4c and d displays the Seebeck output voltage (V) and current (I) with and without BN50-PI50 heat sink membrane at different heating temperatures. As expected, the membrane loaded TE device yields larger voltages and currents. Although the membrane can work at 300 °C, we still set the upper limit of the heating temperature to 220 °C, because of the upper temperature limitation of the commercial TE module. When the hot stage was heated to 220 °C, we could achieve a voltage of ca. 0.71 V and a current of 54 mA, i.e. 34% and 40% enhancements versus the membrane-free device. These results validate the suitability of the BN50-PI50 membrane to enhance heat harvesting and conversion with thermoelectric generators, hence highlighting the high temperature availability. As presented in Fig. 4e, ΔT increases with the hot side temperature. For the BN50-PI50 membrane-loaded TEG, ΔT is nearly twice that under air-cooling, indicating efficient heat dissipation. To confirm the temperature gradient measurement (Fig. S15), we calculated the expected Seebeck voltages of the TEG for such temperature gradients (Fig. S16). The measured values fit well with the expected ones, despite a minor deviation at larger ΔT that is reasonable due to the not regulated ambient surroundings. Encouragingly, the maximum output power from the BN50-PI50-loaded TEG reaches 38.3 mW (Fig. 4f), i.e. 132 % higher than for the air-cooled device (16.5 mW), indicating that additional 21.8 mW power is generated by the BN50-PI50-loaded TEG at 220 °C hot stage heating. Hence, apart from efficient cooling, such temperature differences enable extra power generation. Furthermore, previous membrane cooling efficiency measurements mainly relied on either IR images or digital thermometers [4,6]. In contrast, this conceptual design provides a more practical approach for evaluating the practical heat dissipation ability of a thermal sink.

To further enable the practicability for high temperature cooling and waste heat conversion, we then connected 3 TE modules in series (Fig. 5a) and no any voltage amplifier or power charging subassembly were introduced. Interestingly, the naturally cooled TEG without the heat spreader yielded a total output voltage of only 1.66 V, even under maximum heating temperature at 220 °C (Fig. 5b). By comparison, the assembly of BN50-PI50-membrane loaded TEGs delivers a total output voltage of 1.92 V that is enough to steadily drive a LED bubble (working voltage 1.8 V) and a calculator (Fig. 5c and Fig. S17, Videos S1 and S2). This high voltage was reached far below the maximum operation temperature (220 °C), at 180 °C. This should reduce the cost of the whole energy

conversion process. These encouraging results attributed to the efficient cooling of the thermo-anisotropic BN50-PI50 heat sink membrane, where the nacre-like BN and PI nanostructure dissipates heat in the membrane plane. Meanwhile, the high thermal stability of BN and PI allows for workability in such a hot condition for more cost-effective power conversion, which is applicable for in-plane waste heat utilization under high temperature.

4. Conclusions

In summary, we have successfully designed bio-inspired nacre-like freestanding boron nitride-polyimide nanocomposite membranes. The laminated layered structure of the nanocomposite not only improves the mechanical performances, but also provides superior thermal conductivity along the plane of the membranes. Additionally, the membrane features fire-resistance and high thermal stability in a wide temperature range (30–300 °C), combined with great thermo-anisotropy. These characteristics provide the membrane with high potential for use as a 2D heat sink to cool a variety of electronic components working at high temperatures. For instance, the biomimetic membrane in this work can be highly effective for heat dissipation on the cold side of the TE module even under 220 °C heating, hence improving the planar thermal-to-electrical energy conversion. Therefore, our work provides an effective strategy to fabricate high temperature thermal spreader for efficient waste in-plane heat harvest and conversion.

Funding

This work was financially supported by the Australian Research Council Discovery Program (DP190103290) and Australian Research Council Discovery Early Career Researcher Award scheme(DE150101617 and DE140100716). We also thank the Australian Synchrotron for the SAXS/WAXS beamline (Beam time ID: M13292). D.G. is grateful to the Australian Research Council Laureate Fellowship FL160100089 and QUT Project No. 323000-0355/51.

Declaration of competing interest

The authors declare that they have no known competing financial interests or personal relationships that could have appeared to influence the work reported in this paper.

Appendix A. Supplementary data

Supplementary data to this article can be found online at https://doi.org/10.1016/j.jmat.2020.08.006.

References

[1] Ma R, Zhang Z, Tong K, Huber D, Kornbluh R, Ju Y, Pei Q. Science 2017;357:1130–4.
[2] Song H, Liu J, Liu B, Wu J, Cheng HM, Kang F. Joule 2018;2:442–63.
[3] Zhang Y, Heo Y, Son Y, An K-H, Kim B-J, Park S-J. Carbon 2019;142:445–60.
[4] Wang J, Wu Y, Xue Y, Liu D, Wang X, Hu X, Bando Y, Lei W. J Mater Chem C 2018;6:1363–9.
[5] Wu Y, Xue Y, Qin S, Liu D, Wang X, Hu X, Li J, Bando Y, Golberg D, Chen Y, Gogotsi Y, Lei W. ACS Appl Mater Interfaces 2017;9:43163–70.
[6] Wang J, Li Q, Liu D, Chen C, Chen Z, Yang C, Hao J, Li Y, Zhang J, Naebe M, Lei W. Nanoscale 2018;10:16868–72.
[7] Zeng X, Sun J, Yao Y, Sun R, Xu J, Wong CP. ACS Nano 2018;11:5167–78.
[8] Wu K, Fang J, Ma J, Huang R, Chai S, Chen F, Fu Q. ACS Appl Mater Interfaces 2017;9:30035–45.
[9] Zhang L, Kim T, Li N, Kang T, Chen J, Pringle J, Zhang M, Kazim A, Fang S, Haines C, Al-Masri D, Cola B, Razal J, Di J, Beirne S, MacFarlane D, Martin A, Mathew S, Kim Y, Wallace G, Baughman R. Adv Mater 2017;29:1605652.
[10] Zeng X, Ye L, Yu S, Li H, Sun R, Xu J, Wong CP. Nanoscale 2015;7:6774–81.
[11] Yao Y, Zeng X, Sun R, Xu J, Wong CP. ACS Appl Mater Interfaces 2016;8:15645–53.
[12] Tsai MH, Tseng IH, Chiang JC, Li J. ACS Appl Mater Interfaces 2014;6:8639–45.
[13] Tanimoto M, Yamagata T, Miyata K, Ando S. ACS Appl Mater Interfaces 2013;5:4374–82.
[14] Lei W, Mochalin NV, Liu D, Qin S, Gogotsi Y, Chen Y. Nat Commun 2015;6:8849.
[15] Wang J, Liu D, Li Q, Chen C, Chen Z, Fakhrhoseini S, Naebe M, Song P, Wang X, Lei W. ACS Nano 2019;13:7860–70.
[16] Ha W, Choudhury A, Kamal T, Kim D, Park SY. ACS Appl Mater Interfaces 2012;4:4623–30.
[17] Ling Z, Ren CE, Zhao M, Yang J, Giammarco JM, Qiu J, Barsoum MW, Gogotsi Y. Proc Natl Acad Sci Unit States Am 2014;11:16676–81.
[18] Zhu J, Zhang H, Kotov N. ACS Nano 2013;7:4818–29.
[19] Kotov N. Natl. Sci. Rev. 2017;4:284–5.
[20] Wan S, Li Y, Mu J, Alievc A, Fang S, Kotov N, Jiang L, Cheng Q, Baughman R. Proc Natl Acad Sci 2018;21:5359–64.
[21] Song P, Dai J, Chen G, Yu Y, Fang Z, Lei W, Fu S, Wang H, Chen Z. ACS Nano 2018;12:9266–78.
[22] Wu K, Liao P, Du R, Zhang Q, Chen F, Fu Q. J Mater Chem A 2018;6:11863–73.
[23] Song N, Cui S, Hou X, Ding P, Shi L. ACS Appl Mater Interfaces 2017;9:40766–73.
[24] Zeng H, Wu J, Ma Y, Ye Y, Liu J, Li X, Wang Y, Liao Y, Luo X, Xie X, Mai X. ACS Appl Mater Interfaces 2018;10:41690–8.
[25] Ribeiro H, Trigueiro J, Silva W, Woellner C, Owuor P, Chipara A, Lopes M, Tiwary C, Pedrotti J, Salvatierra C, Tour J, Chopra N, Odeh I, Silva G, Ajayan PM. ACS Appl Mater Interfaces 2017. https://doi.org/10.1021/acsami.7b09945.
[26] Wang X, Wu P. ACS Appl Mater Interfaces 2017;9:19934–44.
[27] Song N, Jiao D, Ding P, Cui S, Tang S, Shi L. J Mater Chem C 2016;4:305–14.
[28] Yao Y, Zeng X, Wang F, Sun R, Xu J, Wong CP. Chem Mater 2016;28:1049–57.
[29] Tian X, Itkis ME, Bekyarova EB, Haddon RC. Sci Rep 2013;3:01710.
[30] Park JG, Cheng Q, Lu J, Bao J, Li S, Tian Y, Liang Z, Zhang C, Wang B. Carbon 2012;50:2083–90.
[31] Gong J, Liu Z, Yu J, Dai D, Dai W, Du S, Li C, Jiang N, Zhan Z, Lin CT. Compos Part A Appl Sci Manuf 2016;87:290–6.
[32] Wan J, Song J, Yang Z, Kirsch D, Jia C, Xu R, Dai J, Zhu M, Xu L, Chen C, Wang Y, Wang Y, Hitz E, Lacey SD, Li Y, Yang B, Hu LB. Adv Mater 2017;29:1703331.
[33] Chen Y, Guo X, Wang J, He W, Silberschmidt VV, Wang S, Tao Z, Xu H. J Appl Polym Sci 2015;132:41889.
[34] Chen J, Huang X, Zhu Y, Jiang P. Adv Funct Mater 2017;27:1604754.
[35] Huang X, Zhi C, Jiang P, Golberg D, Bando Y, Tanaka T. Adv Funct Mater 2013;23:1824–31.
[36] Jin W, Yuan L, Liang G, Gu A. ACS Appl Mater Interfaces 2014;6:14931–44.
[37] Mu E, Wu Z, Wu Z, Chen X, Liu Y, Fu X, Hu Z. Nano energy 2019;55:494–500.
[38] Min P, Liu J, Li X, An F, Liu P, Shen Y, Koratkar N, Yu Z. Adv Funct Mater 2018;28:1805365.
[39] Zhang L, Li R, Tang B, Wang P. Nanoscale 2016;8:14600–7.
[40] Ding T, Zhu L, Wang X, Chan K, Lu X, Cheng Y, Ho G. Adv. Energy Mater. 2018;8:1802397.

Jiemin Wang has achieved his doctoral degree at Institute for Frontier Materials, Deakin University, Australia in Dec. 2019. He also has obtained his Master degree in Dec. 2012 with the major of Polymer Science and Engineering from The University of Manchester, UK and bachelor degree in June 2011 with the major of Polymer Materials Science and Engineering in Sichuan University, China. His current research interests focus on the nanocomposites and porous materials for environmental and energy applications.

Dr Weiwei Lei is a Senior Research Fellow at the Institute for Frontier Materials, Deakin University, Australia. He received his Ph.D. degree from Jilin University in 2009. From 2010 to 2011, he worked as a research fellow at Max Planck Institute of Colloids and Interfaces in Germany. Afterwards, he was awarded an Alfred Deakin Post-doctoral Research Fellowship (2011) and ARC Discovery Early Career Researcher (2014) at Deakin University. His research includes the synthesis of two- and three-dimensional nanomaterials and their applications in sustainable energy and water applications.